Inorganic Chemistry

ARTICLE

pubs.acs.org/IC

Discrimination of Mononuclear and Dinuclear Dinitrosyl Iron Complexes (DNICs) by S K-Edge X-ray Absorption Spectroscopy: Insight into the Electronic Structure and Reactivity of DNICs

Tsai-Te Lu,[†] Szu-Hsueh Lai,[†] Ya-Wen Li,[‡] I-Jui Hsu,*[,‡] Ling-Yun Jang,[§] Jyh-Fu Lee,[§] I-Chia Chen,*[,†] and Wen-Feng Liaw*[,†]

[†]Department of Chemistry, National Tsing Hua University, Hsinchu 30013, Taiwan

[‡]Department of Molecular Science and Engineering, National Taipei University of Technology, Taipei 10608, Taiwan

[§]National Synchrotron Radiation Research Center, Hsinchu 30076, Taiwan

Supporting Information

ABSTRACT: In addition to probing the formation of dinitrosyl iron complexes (DNICs) by the characteristic Fe K-edge pre-edge absorption energy ranging from 7113.4 to 7113.8 eV, the distinct S K-edge pre-edge absorption energy and pattern can serve as an efficient tool to unambiguously characterize and discriminate mononuclear DNICs and dinuclear DNICs containing bridged-thiolate and bridged-sulfide ligands. The higher Fe−S bond covalency modulated by the stronger electron-donating thiolates promotes the Fe → NO π-electron back-donation to strengthen the Fe−NO bond and weaken the NO-release ability of the mononuclear DNICs, which is supported by the Raman ν-(Fe−NO) stretching frequency. The Fe−S bond covalency of DNICs further rationalizes the binding preference of the $\{Fe(NO)_2\}$ motif toward thiolates following the trend of $[SEt]^-$ > $[SPh]^-$ > $[SC_7H_4SN]^-$. The relative d-manifold energy derived from S K-edge XAS as well as the Fe K-edge pre-edge energy reveals that the electronic structure of the $\{Fe(NO)_2\}^9$ core of the mononuclear DNICs $[(NO)_2Fe(SR)_2]^-$ is best described as $\{Fe^{III}(NO^-)_2\}^9$ compared to $[\{Fe^{III}(NO^-)_2\}^9-\{Fe^{III}(NO^-)_2\}^9]$ for the dinuclear DNICs $[Fe_2(\mu\text{-SEt})(\mu\text{-S})(NO)_4]^-$ and $[Fe_2(\mu\text{-S})_2(NO)_4]^{2-}$.

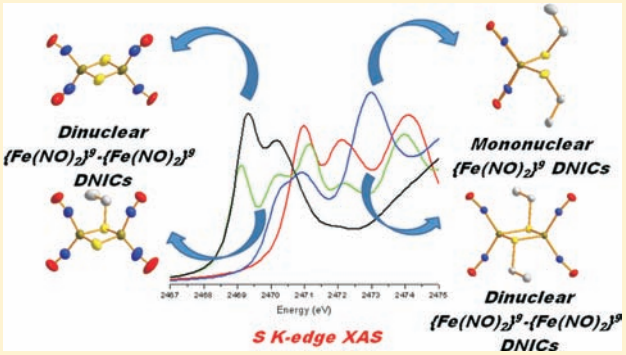

INTRODUCTION

Dinitrosyl iron complexes (DNICs) are one of the two possible forms for storage and delivery of nitric oxide in biological systems.[1] NO can be stored in the form of protein-bound DNICs and is probably released from cells in the form of low-molecular-weight DNICs.[2] DNICs were found to execute the NO-releasing function to result in degradation of the iron−sulfur clusters, S-nitrosylation, vasodilation, activation of cationic channels, inhibition of enzymes, activation of sGC, double-stranded DNA breakage, and triggering the apoptosis of Jurkat cells.[3] It is known that DNICs can be identified by their distinct EPR signals at g = 2.03.[1,2] Actually, simultaneous formation of the mononuclear and dinuclear DNICs was observed upon nitrosylation of the $[4Fe-4S]^{2+}$ clusters of FNR according to EPR and UV−vis spectra.[4a] Although formation of the dinuclear DNICs was observed upon nitrosylation of [Fe−S] or other nonheme iron proteins, unambiguous characterization of dinuclear DNICs in biological systems is limited due to its EPR silence.[4b]

In the previous study, we reported that the NO-releasing ability of DNICs under photolysis is regulated by the thiolate-coordinating ligands.[5] In addition, DNIC $[(NO)_2Fe(SEt)_2]^-$ serves as the thiolate carrier to reduce $[Fe_2(\mu\text{-SEt})_2(NO)_4]$, leading to formation of $[Fe_2(\mu\text{-SEt})_2(NO)_4]^-$, and to activate $HSCPh_3/Me_2S_3$, producing $[Fe_2(\mu\text{-SEt})(\mu\text{-S})(NO)_4]^-$.[6a,b] Mononuclear DNIC $[(NO)_2Fe(S^tBu)_2]^-$ and dinuclear DNIC $[Fe_2(\mu\text{-}S^tBu)_2(NO)_4]$ display the dynamic equilibrium in protic solvent MeOH.[7] The interconversion between mononuclear and dinuclear DNICs via protonation and bridged-thiolate cleavage reactions triggered by incoming thiolate/imidazolate ligands, respectively, was demonstrated.[8] We also reported that the EPR spectrum (the pattern of hyperfine splitting) in combination with IR $\Delta\nu_{NO}$ (the relative position of the ν_{NO} stretching frequencies) may serve as an efficient tool for discrimination of the existence of the anionic/neutral mononuclear and dinuclear DNICs. Moreover, the characteristic Fe K-edge pre-edge peak energy (within the range of 7113.4−7113.8 eV) displayed by $\{Fe(NO)_2\}^9$ DNICs may be adopted to probe formation of DNICs in biological systems.[9] This characteristic $Fe_{1s} \rightarrow Fe_{3d}$ transition energy displayed by the anionic $\{Fe(NO)_2\}^9$ DNICs,

Received: October 19, 2010
Published: May 27, 2011

lying between complexes $[Fe(SPh)_4]^{2-}$ and $[Fe(SPh)_4]^{-}$, also suggested that the electronic structure of the mononuclear $\{Fe(NO)_2\}^9$ DNICs is best described as a resonance hybrid of $\{Fe^{II}(NO)(NO^-)\}^9$ and $\{Fe^{III}(NO^-)_2\}^9$, consistent with the computational study.[10]

Sulfur K-edge X-ray absorption spectroscopy (XAS) is a direct probe to investigate the chemical forms of sulfur (i.e., thiolate, sulfenate, and sulfinate), bonding mode, and covalency of the metal−sulfur bond which modulates the function and activity of the abundant metal−sulfur active sites.[11−16] In transition-metal complexes containing one or more unoccupied d mainfold, the S K-edge is featured by the intense low-energy pre-edge absorption.[11] This pre-edge feature corresponds to a $S_{1s} \rightarrow \psi^*$ transition, where ψ^* is the metal−sulfur antibonding orbital. The intensity (D_0) of the pre-edge transition is given by

$$D_o(S_{1s} \rightarrow \varphi^*) = \text{const}|\langle S_{1s}|r|\varphi^*\rangle|^2 = \frac{\alpha^2 h}{3n} I_3$$

where α^2 represents the contribution of S_{3p} character in the unoccupied or partially occupied orbitals, h is the number of holes in the acceptor orbital, n is the number of sulfur atoms, and I_s is the electric-dipole-allowed $S_{1s} \rightarrow S_{3p}$ transition which depends on the metal−sulfur distance.[11] This rationalization implies the pre-edge intensity may provide a quantitative estimate of the ligand contribution to the unoccupied or partially occupied orbitals derived from M−S bonding. In conclusion, the metal−sulfur covalency could be directly measured by the S K-edge pre-edge absorption intensity.[11] In contrast to the S-centered oxygenation/oxidation of Ni−thiolate complexes toward oxygen, the Ni-centered redox reaction observed in Ni−SOD was attributed to the decrease of S character mixing in the redox-active molecular orbital (RAMO) of the Ni center.[14] In cytochrome P-450, the highly covalent Fe−S bond provides a "push effect" to enhance the basicity of Fe^{III}−hydroperoxo and to trigger subsequent heterocleavage of the O−O bond.[15] Furthermore, we noticed that the Fe−S bond covalency perturbed by the hydrogen-bonding interaction within protein regulates the redox potential of [Fe−S] proteins.[16]

The primary transition at S K-edge XAS is $S_{1s} \rightarrow S_{4p}$ or $S_{1s} \rightarrow S_{X-S\sigma^*/\pi^*}$ (X = C or O), which is sensitive to the Z_{eff} of the sulfur atom.[11] It is noticed that the distinct transition energies between the $S_{1s} \rightarrow S_{C-S\ \sigma^*}$ orbital and the $S_{1s} \rightarrow S_{O-S\sigma^*}$ orbital were adopted to discriminate the thiolate/sulfenate/sulfinate in the Fe-containing nitrile hydratase.[13] The same concept was also utilized to determine the thiolate bonding mode (terminal vs bridging) of complex $Ni_2\{MeN(CH_2NH_2S)_2\}_2$.[14] In this study, S K-edge XAS serving as an efficient tool to identify and distinguish the mononuclear DNICs and dinuclear DNICs containing bridged-thiolate/-sulfide ligands was demonstrated. On the basis of S K-edge XAS, the electronic structures of the $\{Fe(NO)_2\}^9$ core of the mononuclear DNICs and the $[\{Fe(NO)_2\}^9-\{Fe(NO)_2\}^9]$ core of the dinuclear DNICs were assigned. In particular, the intensity of the S K-edge pre-edge absorption peak of the dinuclear DNICs featuring the Fe−S bond covalency and rationalizing the binding preference of the $\{Fe(NO)_2\}$ motif toward thiolates were also delineated.

RESULTS AND DISCUSSION

Investigation of the Electronic Structures of Mononitrosyl Iron Complexes (MNICs) and Dinitrosyl Iron Complexes (DNICs) by S K-Edge XAS. The S K-edge X-ray absorption spectra

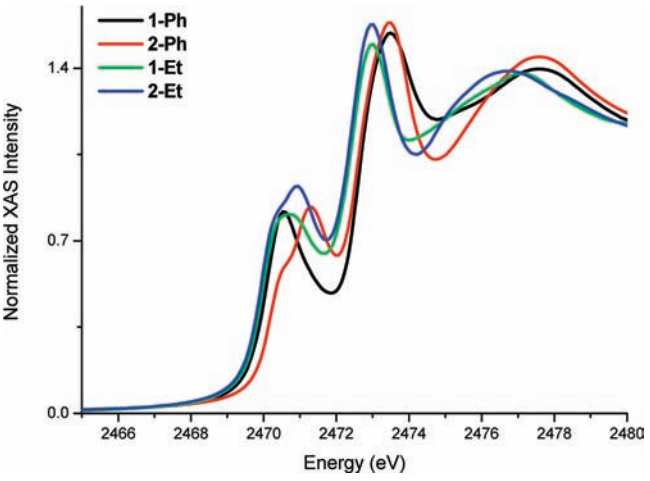

Figure 1. S K-edge spectra of complexes **1-Ph**, **2-Ph**, **1-Et**, and **2-Et**.

Scheme 1

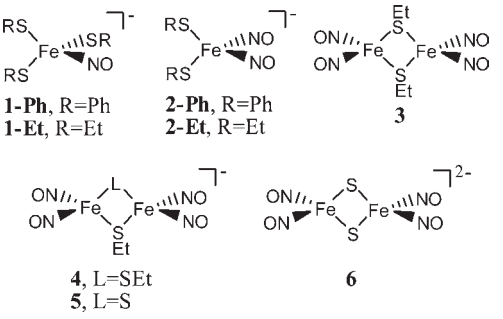

of complexes $[(NO)Fe(SPh)_3]^-$ (**1-Ph**), $[(NO)Fe(SEt)_3]^-$ (**1-Et**), $[(NO)_2Fe(SPh)_2]^-$ (**2-Ph**), and $[(NO)_2Fe(SEt)_2]^-$ (**2-Et**) were depicted in Figure 1 (Scheme 1). Compared to the intense $S_{1s} \rightarrow S_{C-S\sigma^*}$ transition of free $[SR]^-$ (2472.9 eV (R = Ph) and 2472.3 eV (R = Et)), the higher thiolate peak energies of complexes **1-Ph**, **1-Et**, **2-Ph**, and **2-Et** at 2473.5, 2472.9, 2473.5, and 2472.9 eV, respectively, implicate that the significant charge contribution from terminal thiolates to the $\{Fe(NO)\}^7$ core of MNIC and the $\{Fe(NO)_2\}^9$ core of DNIC occurs (Supporting Information Figures S1 and S2). This is consistent with the trend of Mulliken average charge population on S atoms (−0.20, −0.21, −0.22, and −0.31 for $[Fe^{III}(SPh)_4]^-$, **1-Ph**, **2-Ph**, and **2-Et**, respectively). In the S K-edge pre-edge region, complexes **1-Ph**, **1-Et**, **2-Ph**, and **2-Et** exhibit intense pre-edge features (2470.2−2471.3 eV) derived from the $S_{1s} \rightarrow Fe_{3d}$ transition. Since the thiolate peak energy ($S_{1s} \rightarrow S_{C-S\ \sigma^*}$ transition (C−S σ^* orbitals are degenerate for the same thiolate ligand)) has been known to reflect the relative energy of the S_{1s} orbital of [M−S] complexes (M = Fe and Ni),[13,14] the pre-edge energy ($S_{1s} \rightarrow Fe_{3d}$ transition) may be adopted to establish the relative energy of the Fe_{3d} manifold orbitals and to estimate the Z_{eff} of the Fe center of MNICs and DNICs.[17] On the basis of the intensity-weighted average pre-edge energy ($S_{1s} \rightarrow Fe_{3d}$ transition, 2470.2 eV for complex $[Fe(SPh)_4]^-$ and 2470.8 eV for complex **1-Ph**) and thiolate peak energy ($S_{1s} \rightarrow S_{C-S\ \sigma^*}$ transition, 2473.2 eV for complex $[Fe(SPh)_4]^-$ and 2473.5 eV, for complex **1-Ph**) (Table 1), the Fe_{3d} manifold orbital energy of $\{Fe(NO)\}^7$ **1-Ph** is calculated to be 0.3 eV higher than that of complex $[Fe^{III}(SPh)_4]^-$. The relative Fe_{3d} manifold orbital energies of

dx.doi.org/10.1021/ic102108b |Inorg. Chem. 2011, 50, 5396–5406

Table 1. Pre-Edge Energy, Thiolate Peak Energy, and Calculated Relative d-Manifold Energy Shift Derived from S K-Edge XAS

complexes	pre-edge energy (eV)[a]		averaged thiolate pre-edge energy (eV)[b]	thiolate peak energy (eV)[a]	relative d-manifold energy shift (eV)[c]
$[Fe^{II}(SPh)_4]^{2-}$[d]	2471.4		2471.4	2473.3	1.1
$[Fe^{III}(SPh)_4]^{-}$[d]	2470.2		2470.2	2473.2	0
1-Ph	2470.5	2471.3	2470.8	2473.5	0.3
2-Ph	2470.5	2471.3	2471.0	2473.5	0.5

[a] The pre-edge and thiolate peak energies are determined by the minimum of the second derivative. [b] The intensity-weighted average energy is given here. [c] Calculated from the difference of the thiolate peak energy and the intensity-weighted pre-edge peak energy. [d] From ref 17.

Table 2. Pre-Edge Energy, Thiolate Peak Energy, and Calculated Relative d-Manifold Energy Shift Derived from S K-Edge XAS

complexes	pre-edge energy (eV)[a]		averaged thiolate pre-edge energy (eV)[b]	thiolate peak energy (eV)[a]	relative d-manifold energy shift (eV)[c]
$[Fe^{III}(SEt)_4]^{-}$[d]					0
$[(EtS)_2Fe(\mu\text{-}S)]_2^{2-}$[e]	2470.6		2470.6	2472.7	0.5
1-Et	2470.3	2470.9	2470.6	2472.9	0.3
2-Et	2470.2	2470.9	2470.6	2472.9	0.3
3	2470.9	2472.0	2471.4	2474.2	−0.2
4	2470.9	2471.7	2471.4	2473.6	0.4
5	2469.1	2470.1	2471.6	2474.0	0.2
	2471.1	2472.2			
6	2469.3	2470.2			
$[(-SC_7H_4SN)_2Fe(NO)_2]^{-}$	2470.6	2471.4	2470.9	2472.6	
				2473.7	

[a] The pre-edge and thiolate peak energies are determined by the minimum of the second derivative. [b] The intensity-weighted average energy is given here. [c] Calculated from the difference of the thiolate peak energy and the intensity-weighted pre-edge peak energy. [d] The relative d-manifold energy of complex $[Fe^{III}(SEt)_4]^{-}$ is 0.5 eV lower than that of complex $[(EtS)_2Fe(\mu\text{-}S)]_2^{2-}$ on the basis of the theoretical calculation.[17] [e] From ref 18.

complexes $[Fe(SPh)_4]^{2-}$, **1-Ph**, and **2-Ph** (vs $[Fe(SPh)_4]^{-}$) were then calculated and collected in Table 1. As shown in Table 1, the derived relative Fe_{3d} manifold energies implicate that the Fe Z_{eff} of the $\{Fe(NO)\}^7$ MNIC **1-Ph** and the $\{Fe(NO)_2\}^9$ DNIC **2-Ph** lie between those of $[Fe^{II}(SPh)_4]^{-}$ and $[Fe^{III}(SPh)_4]^{2-}$. On the basis of the linear relationship between the oxidation state and the effective nuclear charge Z_{eff} and following the method reported by Sun et al.,[17c] the oxidation state of Fe is estimated to be 2.75 for **1-Ph** and 2.59 for **2-Ph** when the oxidation states of $[Fe^{III}(SPh)_4]^{-}$ and $[Fe^{II}(SPh)_4]^{2-}$ are defined as 3.0 and 2.0, respectively (see Supporting Information). The relative d-manifold energy derived from S K-edge XAS as well as the Fe K-edge pre-edge energy reveal that the electronic structure of the $\{Fe(NO)_2\}^9$ core of the mononuclear DNICs is best described as $\{Fe^{III}(NO^{-})_2\}^9$. We cannot rule out the possibility of formation of a resonance electronic structure of $\{Fe^{III}(NO^{-})_2\}^9$ and $\{Fe^{II}(^{\bullet}NO)(NO^{-})\}^9$ since replacement of two $[SPh]^{-}$ by two NO^{-} in DNICs may change the shielding effect.

According to the theoretical study on the difference (0.512 eV) of the Fe_{3d} manifold orbital energies between $[Fe_2(\mu\text{-}S)_2(SMe)_4]^{2-}$ and $[Fe(SMe)_4]^{-}$,[17] the Fe_{3d} manifold energy of complex $[Fe(SEt)_4]^{-}$ was estimated to be 0.5 eV lower than that of complex $[Fe_2(\mu\text{-}S)_2(SEt)_4]^{2-}$. Adopting the approach described above to derive the relative Fe_{3d} manifold energies of complexes **1-Ph** and **2-Ph** (vs complex $[Fe(SPh)_4]^{-}$), the Fe_{3d} manifold orbital energies of complexes **1-Et** and **2-Et** are then calculated to be higher than that of $[Fe(SEt)_4]^{-}$ by 0.3 eV (Table 2).

Correlation of the Quantitative Analysis of Fe−S Bond Covalency of DNICs to Their Physical Property and Chemical Reactivity. As presented above, the S K-edge pre-edge and thiolate peak energies of **2-Ph**/**2-Et** were demonstrated to provide a superior level of insight on elucidating the electronic structure of the $\{Fe(NO)_2\}^9$ core of DNICs. It is noticed that the intensity of the pre-edge is known to serve as a probe of the ligand character of the unoccupied or partially occupied orbitals and a probe of Fe−S bond covalency.[11] As shown in Figure 2, two pre-edge absorption peaks at 2470.2 and 2470.9 eV for complex **2-Et** (2470.5, 2471.3 eV for complex **2-Ph** and 2470.6, 2471.4 eV for complex $[(-SC_7H_4SN)_2Fe(NO)_2]^{-}$, respectively) were observed. In order to resolve the pre-edge feature of complexes **2-Et**, **2-Ph**, and $[(-SC_7H_4SN)_2Fe(NO)_2]^{-}$, TD-DFT calculations were conducted. The MO diagrams of the unoccupied orbitals of

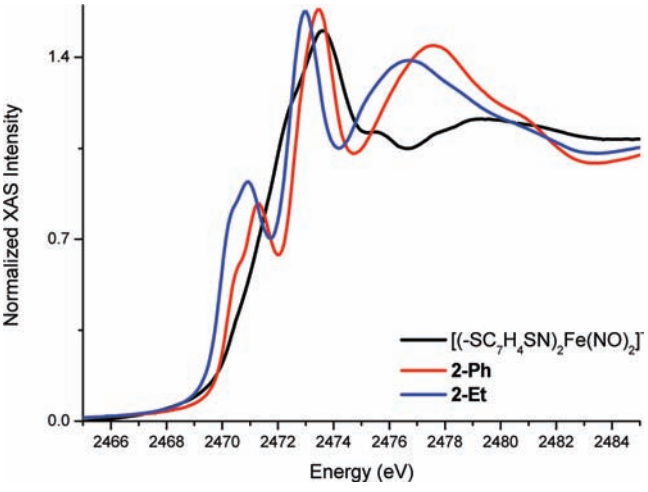

Figure 2. S K-edge spectra of complexes $[(-SC_7H_4SN)_2Fe(NO)_2]^{-}$, **2-Ph**, and **2-Et**.

dx.doi.org/10.1021/ic102108b |*Inorg. Chem.* 2011, 50, 5396–5406

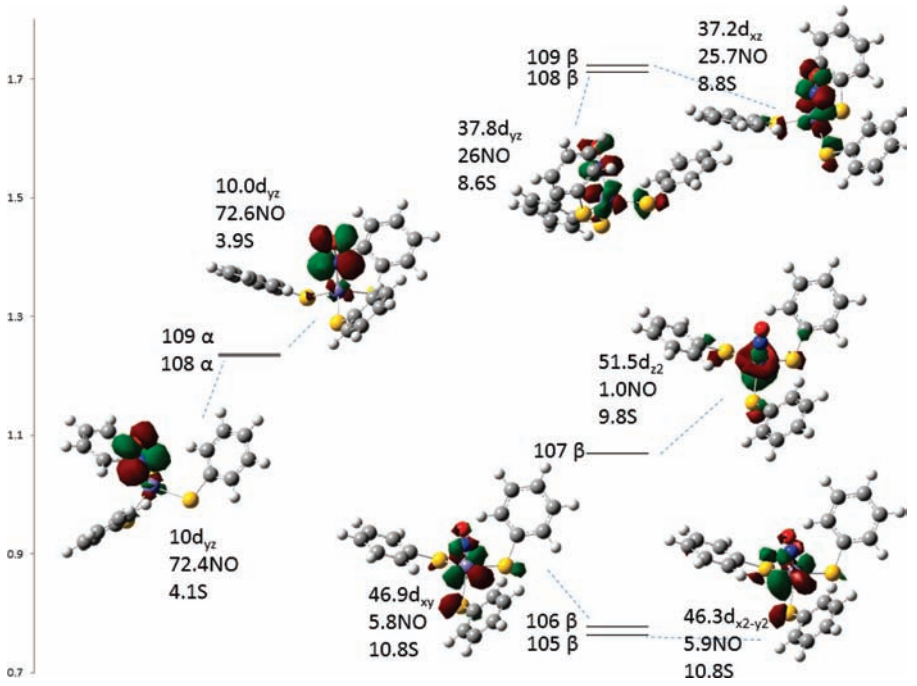

Figure 3. Unoccupied MO diagram of complex **1-Ph**. Numbers shown are the percentage of Fe 3d, NO 2p, and S 3p orbitals in each MO.

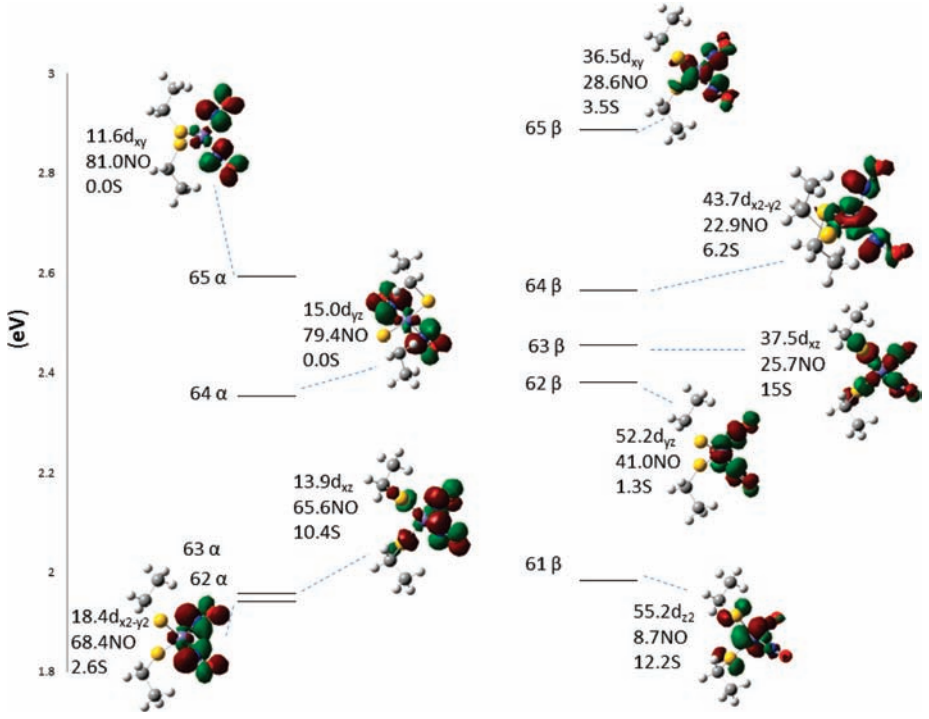

Figure 4. Unoccupied MO diagram of complex **2-Et**. Numbers shown are the percentage of Fe 3d, NO 2p, and S 3p orbitals in each MO.

mononuclear iron nitrosyl complexes **1-Ph**, **2-Et**, and **2-Ph** are displayed in Figures 3, 4, and S3, Supporting Information, respectively, and the composition of these orbitals is also listed. As shown in Figure 3, the two unoccupied α orbitals 108−109 are NO π^* orbitals and the five unoccupied β orbitals 105−109 all have dominant d character of Fe. That is, the Fe 3d orbitals have five α electrons while the NO π^* orbitals have two β electrons. The Mulliken spin densities are 3.34 and −1.03 on Fe and NO, respectively. Therefore, complex **1-Ph** may be described as high-spin Fe^{III} ($S = 5/2$) antiferromagnetically coupled to one triplet NO^- ($S = 1$) to yield $S_{total} = 3/2$ in such $\{Fe(NO)\}^7$ system. A detailed discussion on this system has been reported by Conradie et al.[6c] and other groups.[6d−f] In complex **2-Et**, there are four unoccupied α orbitals 62−65 derived from NO π^* orbitals and

dx.doi.org/10.1021/ic102108b |*Inorg. Chem.* 2011, 50, 5396–5406

five unoccupied β orbitals 61−65 dominant from the d character of Fe. This implies that the Fe 3d orbitals have five α electrons and the NO π^* orbitals have four β electrons. The Mulliken spin density is 2.75 on Fe and −1.03 on each NO. The electronic structure of the $\{Fe(NO)_2\}$ core of complex **2-Et** is then described as high-spin Fe^{III} (S = 5/2) antiferromagnetically coupled to two triplet NO^- (S = 1) to yield S_{total} = 1/2 in the $\{Fe(NO)_2\}^9$ system.[9] We also noticed that the delocalization between Fe 3d and NO π^* in the β unoccupied orbitals reflects the electron donation from the occupied NO^- π^* to the Fe 3d orbitals, and the delocalization between NO π^* and Fe 3d in the α unoccupied orbitals reflects the backbonding of the occupied Fe 3d character into the NO π^* orbitals.[17c] The amount of electron donation from the NO π^* orbitals to Fe 3d is ∼64%, ∼129%, and ∼127% for **1-Ph**, **2-Ph**, and **2-Et**, respectively, while the electron back-donation from Fe 3d to NO π^* is ∼20%, ∼57%, and ∼59% for **1-Ph**, **2-Ph**, and **2-Et**, respectively. The larger amount of electron donation from NO π^* to Fe 3d for **2-Ph** compared to **1-Ph** somewhat decreases the Z_{eff} of the Fe^{III} center. This rationalizes that the oxidation state of Fe, estimated from S K-edge data, is 2.75 for **1-Ph** and 2.59 for **2-Ph**.

On the basis of ligand field theory, the d manifold will be split into e and t_2 states with an energy difference $10Dq$ when a pseudotetrahedral environment around the Fe center of $[Fe^{III}(SPh)]^-$, **1-Ph,** and **2-Ph** is assumed. The S K-edge pre-edge energy is the contribution with transitions S 1s → e and S 1s → t_2. The energy difference between e and t_2 is ∼0.4 and ∼0.8 eV in complexes $[Fe^{III}(SPh)_4]^-$ and **1-Ph**, respectively. This result indicates that NO^- will induce stronger ligand field splitting compared to that of $[SPh]^-$ ligand. However, this splitting energy is almost the same as that of **2-Ph** (Table 1). This may be attributed to the improper assumption of a T_d environment in **2-Ph**. As Shadle et al. pointed out,[17d] the distortion from T_d to D_{2d} has a non-negligible effect on the metal d-derived energies in that the t_2 set will be split into e + b_2. The higher pseudo-symmetry C_{2v} point group may be the proper symmetry in describing DNICs, although the real molecule should be classified as a C_1 point group. If we take the multiplets into such pseudo-T_d systems, d^5 of Fe^{III} has ground state $^6A_1$ and two excited parent states ^5E and $^5T_2$, which are associated to transitions to the e and t_2 states, respectively. Qualitatively, we observed two transition peaks from the pre-edge region. However, it will be quite complicated on going to lower symmetry. It is noticed that the paper published by Sun et al. presented a more detailed discussion about the effects of the ligand field and multiplets on the S K-edge spectra.[17c,d] In the following discussion about TD-DFT results, all molecules are calculated in C_1 symmetry except that C_i is used in complex **3**.

The experimental and calculated S K-edge pre-edge absorption spectra of mononuclear iron nitrosyl complexes **1-Ph**, **2-Et**, **2-Ph**, and $[(-SC_7H_4SN)_2Fe(NO)_2]^-$ are depicted in Figures 5, 6, S4, Supporting Information, and S5, Supporting Information, respectively. On the basis of the TD-DFT calculations, the two pre-edge absorption peaks observed in the S K-edge spectrum of complex **1-Ph** are attributed to the S_{1s} to 105β, 106β, 107β, 108α/109α, and 108β/109β transitions. The transitions from S_{1s} to 105β and 106β are related to the Fe−S π^* antibonding characters, and the transitions from S_{1s} to 108 and 109 correspond to S_{1s} → Fe−S σ^* antibonding orbitals. In complex **2-Et**, the two pre-edge absorption peaks are ascribed to transitions from S_{1s} to 61β, 63α, and 63β. The transition from S_{1s} to 61β is related to the Fe−S π^* antibonding orbitals, and the transitions from S_{1s} to 63α and 63β correspond to S_{1s} → Fe−S σ^* antibonding orbitals. Similarly, the combination of the S_{1s} → 85β, S_{1s} → 86α, and S_{1s} → 87β transitions results in the pre-edge feature of complex **2-Ph** (Figure S4, Supporting Information), whereas the pre-edge feature of complex $[(-SC_7H_4SN)_2Fe(NO)_2]^-$ exhibits the combined S_{1s} → 113β, S_{1s} → 114α, and S_{1s} → 115β transitions (Figure S5, Supporting Information). Accordingly, the S K-edge spectra of complexes **2-Et**, **2-Ph**, and $[(-SC_7H_4SN)_2Fe(NO)_2]^-$ were

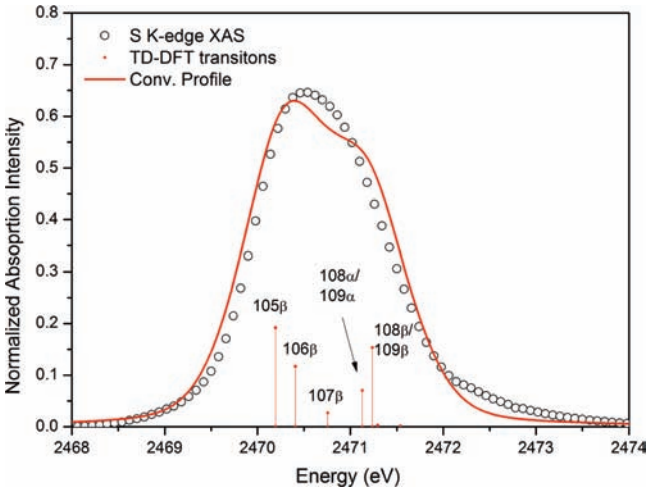

Figure 5. Experimental (○) and TD-DFT-calculated (red solid line) pre-edge absorption of complex **1-Ph**. The theoretically calculated transition peaks are displayed in the vertical lines. All transitions have been convolved with a pseudo-Voigt function with 1:1 ratio of Lorentzian to Gaussian and of 0.45 eV half-width to account for experimental and core−hole broadening. The transition energy is shift by 40.4 eV to get better agreement between the experimental and the calculated profile.

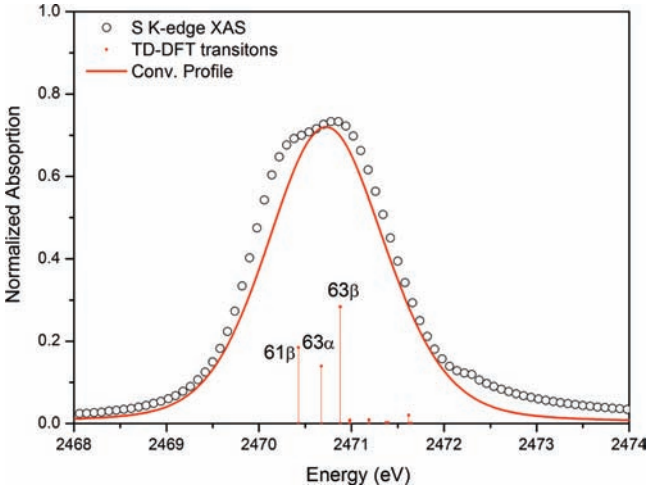

Figure 6. Experimental (○) and TD-DFT-calculated (red solid line) pre-edge absorption of complex **2-Et**. The theoretically calculated transition peaks are displayed in the vertical lines. All transitions have been convolved with a pseudo-Voigt function with a 1:1 ratio of Lorentzian to Gaussian and of 0.6 eV half-width to account for experimental and core-hole broadening. The transition energy is shift by 40.5 eV to get better agreement between the experimental and the calculated profile.

dx.doi.org/10.1021/ic102108b |*Inorg. Chem.* 2011, 50, 5396–5406

Table 3. S Character in the SOMO, Total Covalency, Vibrational Frequencies (cm^{-1}), and Selected Bond Distances (Å) of DNICs 2-Et, 2-Ph, and $[(-SC_7H_4SN)_2Fe(NO)_2]^-$

					ν_s(NO)		ν_{as}(NO)		ν_{as}(N−Fe−N)		ν_s(N−Fe−N)		δ_s(N−Fe−N)	
	% S_{3p} SOMO	total covalency	Fe−S	Fe−N	^{14}NO	^{15}NO	^{14}NO	^{15}NO	^{14}NO	^{15}NO	^{14}NO	^{15}NO	^{14}NO	^{15}NO
2-Et[b]	26 ± 2	82 ± 8	2.273	1.676	1715	1682	1674	1640	625	620	568	563	482	469
2-Ph	15 ± 1	57 ± 5	2.280[c]	1.679[c]	1737	1694	1693	1661	598[d]	594[d]	525[d]	519[d]	440[d]	429[d]
$[(-SC_7H_4SN)_2Fe(NO)_2]^-$[e]	5 ± 1	20 ± 2	2.294	1.684	1766	1732	1716	1682	535	530	472	466	436	422

[a] % S_{3p} was determined using the reference complex $[Fe(SPh)_4]^-$.[11] [b] From ref 19. [c] From ref 20. [d] From ref 21. [e] From ref 5.

fitted to determine the contribution (percentage) of S_{3p} in the unoccupied orbitals of complexes **2-Et**, **2-Ph**, and $[(-SC_7H_4SN)_2Fe(NO)_2]^-$ and to estimate the Fe−S bond covalency. The renormalized intensities of the pre-edge features of complex **2-Et** are calculated to be 0.21 and 0.45 units (referring to the intensity of the pre-edge feature of complex $[Fe(SPh)_4]^-$ defined as 1.03 unit, 128% total covalency),[11] deducing 26% S_{3p} character and 82% total covalency in complex **2-Et**. The Fe−S bond covalency following the trend of **2-Et** (82%) > **2-Ph** (57%) > $[(-SC_7H_4SN)_2Fe(NO)_2]^-$ (20%) illustrates that complex **2-Et** exhibits the shortest Fe−S bond distance among these complexes (Table 3). Also, the higher Fe−S bond covalency of complex **2-Et**, relative to those of complexes **2-Ph** and $[(-SC_7H_4SN)_2Fe(NO)_2]^-$, may explain why the binding preference of the electron-deficient $\{Fe(NO)_2\}$ motif toward thiolates follows the order of the ligand-displacement reaction of DNICs ($[SEt]^-$ > $[SPh]^-$ > $[SC_7H_4SN]^-$). This is also consistent with the trend of Mulliken average charge population on S atoms with −0.31, −0.22, and −0.10 in **2-Et**, **2-Ph**, and $[(-SC_7H_4SN)_2Fe(NO)_2]^-$, respectively. That is, the stronger electron-donating thiolate $[RS]^-$, compared to the coordinated thiolates of DNIC $[(R'S)_2Fe(NO)_2]^-$, promotes ligand exchange to yield the stable DNIC $[(RS)_2Fe(NO)_2]^-$ in the reaction of complexes $[(R'S)_2Fe(NO)_2]^-$ and $[RS]^-$.[5] In spite of the inherent differences of the reducing ability between $[SEt]^-$ and $[SPh]^-$, the higher sulfur character observed by S K-edge XAS of complex **2-Et** may rationalize that mononuclear DNIC **2-Et** acts as a thiolate carrier to reduce dinuclear DNIC $[Fe_2(\mu\text{-SEt})_2(NO)_4]$ (**3**) to yield $[Fe_2(\mu\text{-SEt})_2(NO)_4]^-$ (**4**) when DNIC **2-Et** was dissolved in protic solvent MeOH.[6a] This explanation further elucidates that mononuclear DNIC **2-Et** serves as thiolate carrier to activate $HSCPh_3$, producing complex $[Fe_2(\mu\text{-SEt})(\mu\text{-S})(NO)_4]^-$ (**5**) in the reaction of complex **2-Et** and $HSCPh_3$ observed in the previous study.[6b]

The very close transition intensity of $Fe_{1s} \rightarrow Fe_{3d}$ observed in Fe K-edge XAS of complexes **2-Et** and **2-Ph** suggests a similar contribution of Fe_{3d} in complexes **2-Et** and **2-Ph**.[9] The larger S_{3p} contribution of complex **2-Et** compared to that of complex **2-Ph** may suggest a lower contribution of the NO ligand to the unoccupied orbitals of complex **2-Et** compared to that of complex **2-Ph**. This result may rationalize the EPR spectrum of complex **2-Ph** displaying a well-resolved five-line hyperfine splitting with A_{NO} = 2.7 G, in contrast to the isotropic EPR signal observed in complex **2-Et**.[5,19] In our previous report we demonstrated that $\{Fe(NO)_2\}^9$ DNICs containing the less electron-donating thiolate ligands displayed a higher NO-release ability (NO-releasing rate $[(-SC_7H_4SN)_2Fe(NO)_2]^-$ > **2-Ph**).[5] Obviously, the Fe−S bond covalency of DNICs regulated by the distinct electron-donating thiolates may modulate the Fe−NO bonding interaction

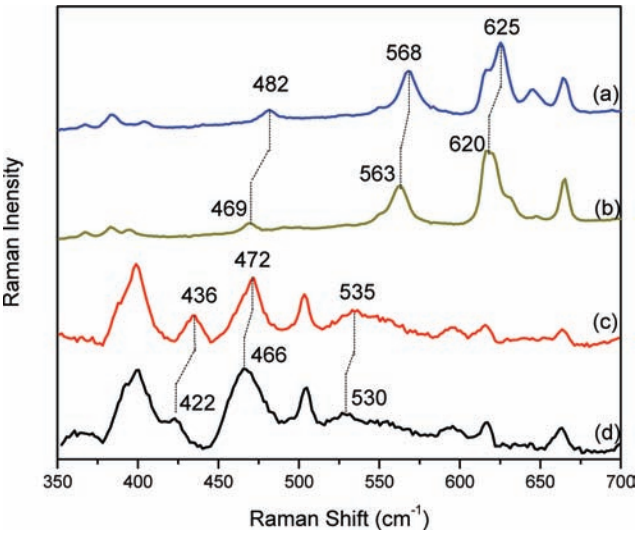

Figure 7. Raman spectra of (a) complex **2-Et**, (b) ^{15}NO-enriched complex **2-Et**, (c) complex $[(-SC_7H_4SN)_2Fe(NO)_2]^-$, and (d) complex $[(-SC_7H_4SN)_2Fe(^{15}NO)_2]^-$. An excitation wavelength of 632.8 nm and a power of 15 mW were used.

and the NO-release ability. The influence of Fe−S bond covalency on the Fe−NO bonding interaction was further elucidated by Raman spectroscopic study on the Fe−NO stretching frequencies of complexes $[(-SC_7H_4SN)_2Fe(NO)_2]^-$, **2-Ph**, and **2-Et**.

Elucidation of the Fe−NO Bonding Interaction in DNICs 2-Et and $[(-SC_7H_4SN)_2Fe(NO)_2]^-$ by Raman Spectroscopy. Correlation between ν(Fe-NO) and ν(N−O) stretching frequencies in the $\{Fe(NO)_2\}^9$ DNICs investigated by Raman spectroscopy was established to delineate the bonding interaction between Fe and NO. As shown in Figure 7, three ^{15}N isotope-sensitive bands at 620, 563, and 469 cm^{-1} observed in the ^{15}NO-enriched **2-Et** (530, 466, and 422 cm^{-1} observed in complex $[(-SC_7H_4SN)_2Fe(^{15}NO)_2]^-$) are assigned as an asymmetric ν(Fe−NO) stretching mode, a symmetric ν(Fe−NO) stretching mode, and a δ(N−Fe−N) bending mode, respectively (Table 3).[21] The ν(Fe−NO) stretching frequencies following the trend of **2-Et** (625, 568 cm^{-1}) > **2-Ph** (598, 525 cm^{-1})[21] > $[(-SC_7H_4SN)_2Fe(NO)_2]^-$ (535, 472 cm^{-1}) support that complex **2-Et** displays the shortest Fe−N bond distance (1.676 Å) among these DNICs (Table 3). As shown in Figure 8, the negative correlation between symmetric ν(Fe−NO) and ν(N−O) stretching frequencies demonstrated that the π-back-bonding interaction between Fe and NO dominated in the $\{Fe(NO)_2\}^9$ DNICs. Also, the positive correlation between Fe−S bond

dx.doi.org/10.1021/ic102108b |*Inorg. Chem.* 2011, 50, 5396–5406

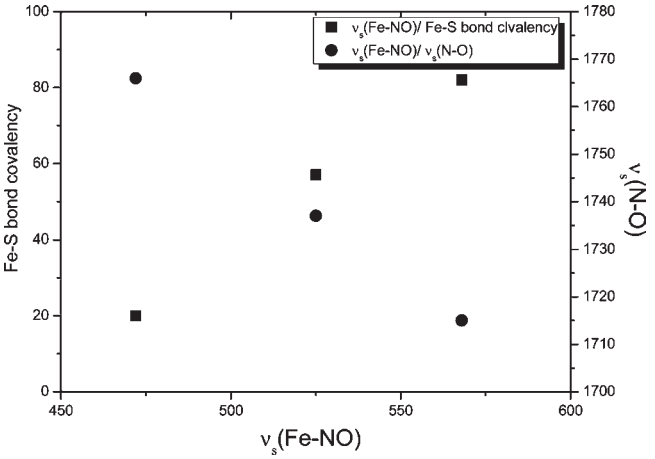

Figure 8. Experimental correlations of ν_s(Fe−NO)/ν(N−O) and ν_s(Fe−NO)/Fe−S bond covalency among complexes $[(-SC_7H_4SN)_2Fe(NO)_2]^-$, **2-Ph**, and **2-Et**.

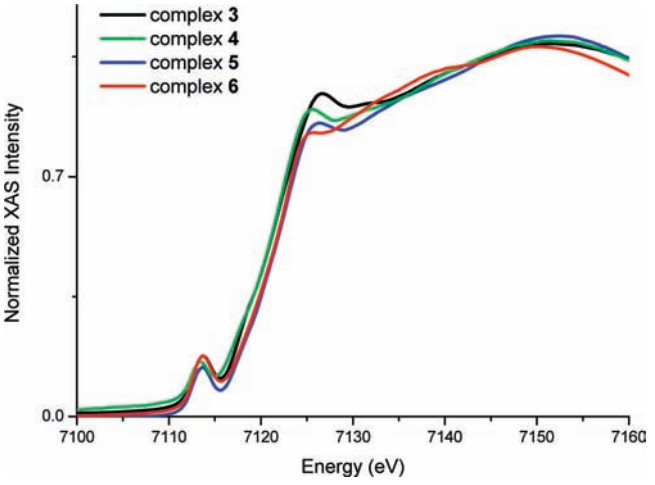

Figure 9. Fe K-edge spectra of complexes **3**, **4**, **5**, and **6**.

Table 4. Pre-Edge Energy of Fe Complexes Derived from Fe K-Edge XAS

complexes	pre-edge energy (eV)
$[Fe^{II}(SPh)_4]^{2-a}$	7112.5
$[Fe^{III}(SPh)_4]^{-a}$	7113.8
2-Ph[a]	7113.5
2-Et[a]	7113.5
3[b]	7113.8
4[b]	7113.4
5	7113.6
6	7113.6

[a] From ref 9. [b] From ref 6a.

covalency and symmetric ν(Fe−NO) stretching frequencies implicates that the higher Fe−S bond covalency modulated by the stronger electron-donating ethylthiolate ligand stabilizes the $\{Fe(NO)_2\}$ core of $\{Fe(NO)_2\}^9$ DNICs and promotes Fe → NO π-electron back-donation to strengthen the Fe−NO bonds of DNIC **2-Et**.

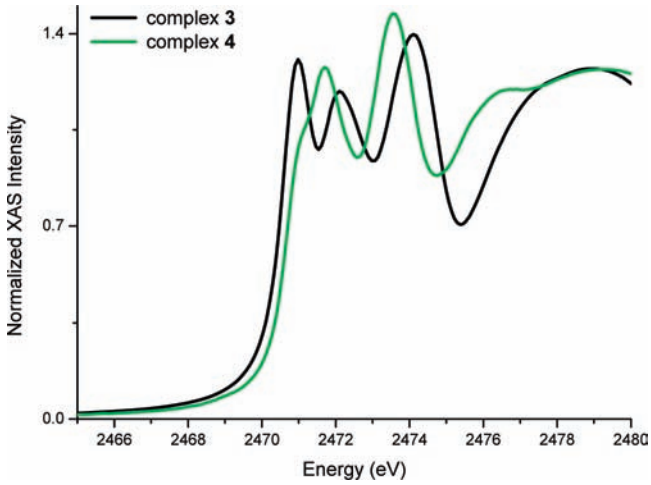

Figure 10. S K-edge spectra of complexes **3** and **4**.

Discrimination of Dinuclear DNICs $[Fe_2(\mu\text{-SEt})_2(NO)_4]$ (3), $[Fe_2(\mu\text{-SEt})_2(NO)_4]^-$ (4), $[Fe_2(\mu\text{-SEt})(\mu\text{-S})(NO)_4]^-$ (5) and $[Fe_2(\mu\text{-S})_2(NO)_4]^{2-}$ (6). The Fe K-edge spectra of complexes $[Fe_2(\mu\text{-SEt})_2(NO)_4]$ (**3**), $[Fe_2(\mu\text{-SEt})_2(NO)_4]^-$ (**4**), $[Fe_2(\mu\text{-SEt})(\mu\text{-S})(NO)_4]^-$ (**5**), and $[Fe_2(\mu\text{-S})_2(NO)_4]^{2-}$ (**6**) are shown in Figure 9 (Scheme 1). The pre-edge energy ($Fe_{1s} \rightarrow Fe_{3d}$ transition) of 7113.6 eV for complexes **5** and **6** lies between those of complex **3** (7113.8 eV) and complex **4** (7113.4 eV) (Table 4). Obviously, the Fe K-edge pre-edge energy might be adopted to serve as a tool to probe the existence of dinuclear $\{Fe(NO)_2\}^9$−$\{Fe(NO)_2\}^9$ and $\{Fe(NO)_2\}^9$−$\{Fe(NO)_2\}^{10}$ DNICs. Compared to the previous report of mononuclear DNICs containing a variety of ligation modes exhibiting the characteristic pre-edge energy falling in the range of 7113.4−7113.8 eV,[9] the pre-edge energy derived from the $Fe_{1s} \rightarrow Fe_{3d}$ transition in a distorted T_d environment of the Fe center falling within the range of 7113.4−7113.8 eV for dinuclear DNICs can be also concluded.

The S K-edge spectra of complexes **3** and **4** are depicted in Figure 10. Due to the increasing effective nuclear charge of sulfur from a terminal thiolate to a bridging thiolate,[17] the shift of the $S_{1s} \rightarrow S_{C-S\sigma^*}$ transition energy from 2472.9 (complex **2-Et**) to 2474.2 eV (complex **3**) was observed (Figures 2 and 9). In contrast to the S K-edge pre-edge absorption peak (2470.9 eV) with a shoulder (2470.2 eV) observed in complex **2-Et**, the S K-edge spectrum of complex **3** showed two well-resolved pre-edge absorption peaks at 2470.9 and 2472.0 eV. These results implied that the unique S K-edge pre-edge pattern/energy and the distinct $S_{1s} \rightarrow S_{C-S\sigma^*}$ transition energy for mononuclear and dinuclear DNICs, respectively, provide the opportunity to distinguish mononuclear DNICs from dinuclear DNICs.

In exploring the electronic structure of the $[\{Fe(NO)_2\}^9$−$\{Fe(NO)_2\}^9]$ core of dinuclear DNIC **3**, the $S_{1s} \rightarrow Fe_{3d}$ (pre-edge peak) and $S_{1s} \rightarrow S_{C-S\sigma^*}$ (thiolate peak) transition energies of complex **3** and complex **2-Et** were taken into comparison. The average pre-edge absorption energy and thiolate peak energy of complex **3** (2471.4 and 2474.2 eV, respectively) and complex **2-Et** (2470.6 and 2472.9 eV, respectively) explain the lower Fe_{3d} manifold energy of complex **3** by 0.5 eV (Table 2). This difference of the Fe_{3d} manifold energy may implicate that the effective nuclear charge of Fe in complex **3** is higher than that of complex **2-Et**. That is, the electronic structure of the $\{Fe(NO)_2\}^9$−$\{Fe(NO)_2\}^9$ core of

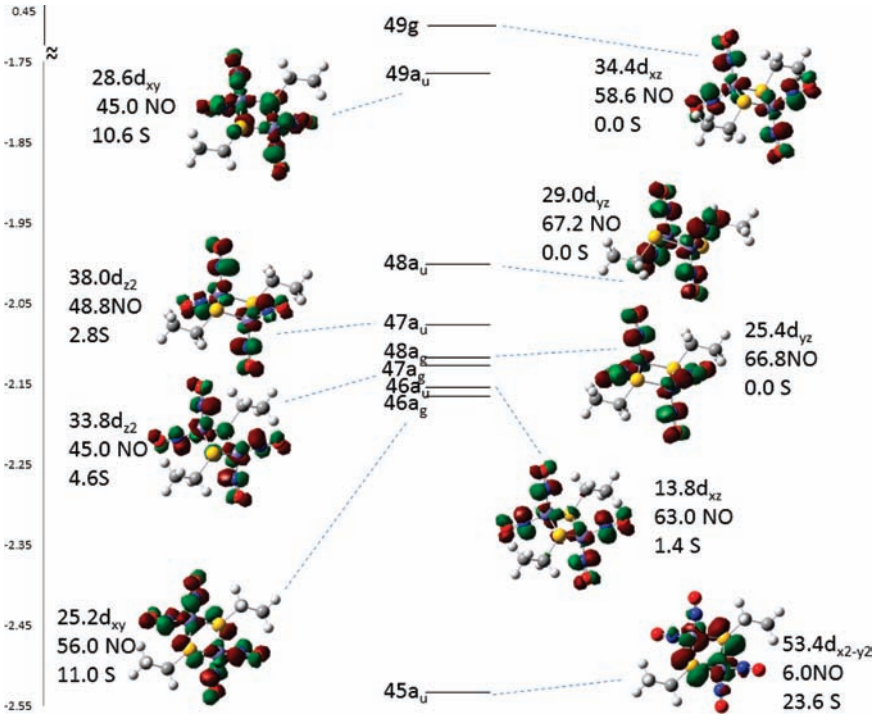

Figure 11. Unoccupied MO diagram of complex **3**. Numbers shown are the percentage of Fe d, NO 2p, and S 3p orbitals in each MO.

complex **3** is best described as $[\{Fe^{III}(NO^-)_2\}^9-\{Fe^{III}(NO^-)_2\}^9]$ ($S = 0$).

As shown in Figure 10, the $S_{1s} \rightarrow Fe_{3d}$ and $S_{1s} \rightarrow S_{C-S\sigma^*}$ transition energies of complex **4** (2471.4 and 2473.6 eV) and complex **3** (2471.4 and 2474.2 eV) indicated the simultaneous increase of the S_{1s} and Fe_{3d} manifold orbital energies by 0.6 eV, respectively (Table 2). The MO diagram of unoccupied orbitals of complex **3** is displayed in Figure 11, and the corresponding contributions of Fe_{3d}, S, and NO are also indicated. The experimental and calculated S K-edge pre-edge absorption spectra of complex **3** are depicted in Figure 12. On the basis of the TD-DFT calculation, the two observed pre-edge absorption peaks are attributed to the S_{1s} to $45a_u$ (LUMO), $46a_g$, and $49a_u$ transitions. Although the transition to the $46a_g$ orbital is parity forbidden (or Larporte forbidden), the S_{3p} orbitals bring out the allowed intensity. Moreover, the major contribution of LUMO is obviously from both Fe atoms and its bound S ligands. Thus, the pre-edge absorption peaks of 2470.9 and 2472.0 eV for complex **3** are attributed to the transition from the S_{1s} to the Fe−S antibonding orbital and to the antibonding orbital mainly contributed from S, NO, and Fe_{3d} orbitals.[6a] The lower intensity of the first pre-edge absorption peak (2470.9 eV) of complex **4**, compared to that of complex **3**, indicates the introduced one electron occupied the LUMO of complex **3** (i.e., the SOMO in complex **4**), as reported by Lu et al.[6a] Since the LUMO is mainly the antibonding character between the Fe−S bond and Fe···Fe, the distances of Fe−S bonds increases from 2.2585(5) (complex **3**) to 2.2965(6) Å (complex **4**). Meanwhile, the Fe···Fe distance increases from 2.7080(5) to 2.8413(6) Å in comparison with the X-ray crystallographic data of complexes **3** and **4**. Elongation of the Fe−S bond will simultaneously increase the S_{1s} and Fe_{3d} orbital energies upon reduction of complex **3** and uncover the reaction of complex **3** and $[SEt]^-$ leading to formation of DNIC $[(NO)_2Fe(SEt)_2]^-$ via the bridged-thiolate cleavage reaction.[6a]

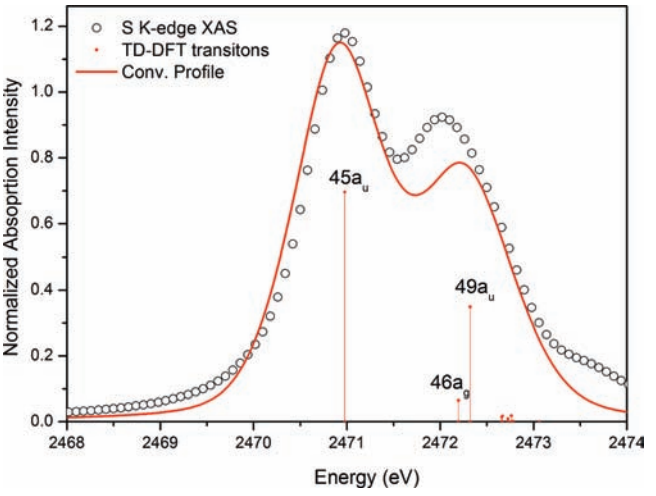

Figure 12. Experimental (○) and TD-DFT-calculated (red solid line) pre-edge absorption of complex **3.** The theoretically calculated transition peaks are displayed in the vertical lines. All transitions have been convolved with a pseudo-Voigt function with a 1:1 ratio of Lorentzian to Gaussian and of 0.5 eV half-width to account for experimental and core−hole broadening. The transition energy is shifted by 40.35 eV to get better agreement between the experimental and the calculated profile.

As shown in Figure 13, compared to two well-resolved pre-edge features (2470.9 and 2472.0 eV) assigned to the transition of S_{1s} of the thiolate ligand to the LUMO of complex **3**, the S K-edge spectrum of complex **6** exhibits two well-resolved pre-edge peaks (2469.3 and 2470.2 eV) assigned to the transition of S_{1s} of the sulfide ligand to the LUMO of complex **6**.[17,18] In combination with the S K-edge energy of complexes **3** and **6**, the dinuclear $\{Fe(NO)_2\}^9-\{Fe(NO)_2\}^9$ DNIC featuring

dx.doi.org/10.1021/ic102108b |*Inorg. Chem.* 2011, 50, 5396–5406

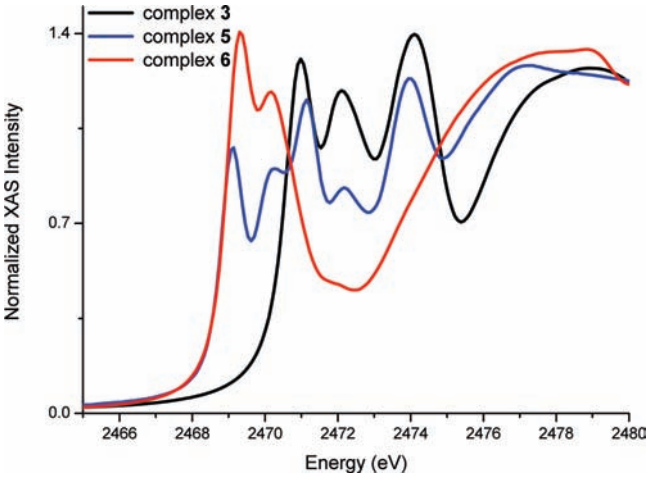

Figure 13. S K-edge spectra of complexes **3**, **5**, and **6**.

the pre-edge energy and pattern (2469.1, 2470.1, 2471.1, and 2472.2 eV), the superposition of thiolate and sulfide contributions in S K-edge pre-edge region[17a] may be also adopted to characterize the mixed-thiolate−sulfide-bridged Roussin's red ester (RRE) **5** (Figure 13).[6b] Obviously, the S K-edge pre-edge pattern/energy may be utilized as a criteria to discriminate the diamagnetic dinuclear DNICs containing bridging sulfide/thiolate ligands, i.e., RRE **3**, mixed-thiolate−sulfide-bridged RRE **5** and Roussin's red salt (RRS) **6**.

Also, it is noticed that the Fe_{3d} manifold energy of complex **5** was calculated to be 0.4 eV higher than that of complex **3** upon changing one bridging thiolate ligand into the stronger electron-donating sulfide ligand. On the basis of the Fe K-edge pre-edge energy (complex **3** (7113.8 eV) > complex **5** (7113.6 eV) ≈ complex **6** (7113.6 eV), displayed in Table 4) and the relative d-manifold energy (complex **5** (0.2 eV) > complex **3** (−0.2 eV) vs $[Fe(SEt)_4]^-$, displayed in Table 2) of complexes **3**, **5**, and **6**, we concluded that the electronic structure of the $[\{Fe(NO)_2\}^9-\{Fe(NO)_2\}^9]$ core of complexes **5** and **6** is best described as $[\{Fe^{III}(NO^-)_2\}^9-\{Fe^{III}(NO^-)_2\}^9]$, compared to the $[\{Fe^{III}(NO^-)_2\}^9-\{Fe^{III}(NO^-)_2\}^9]$ core electronic structure of complex **3**. In addition, both Fe K-edge XAS and the Fe_{3d} manifold energy derived from the S K-edge XAS indicated that the effective nuclear charge of Fe in this series of DNICs follows the trend of complex **3** > complex **2-Et** > complex **5** > complex **4** (Tables 2 and 4), albeit the energy differences of Fe K-edge XAS of these DNICs are smaller than the resolution of Fe K-edge XAS.

■ CONCLUSION AND COMMENTS

A study of S K-edge and Fe K-edge XAS of mononuclear MNICs **1-Ph**/**1-Et**, DNICs **2-Ph**/**2-Et**, and dinuclear DNICs **3**, **4**, **5**, and **6** led to the following results.

(1) In contrast to the S K-edge pre-edge absorption peak (2470.9 eV) with a shoulder (2470.2 eV) observed in mononuclear DNIC **2-Et**, dinuclear DNICs **3** and **6** display two well-resolved pre-edge features assigned to the transition of S_{1s} of the thiolate ligand (2470.9 and 2472.0 eV) and S_{1s} of the sulfide ligand (2469.3 and 2470.2 eV) to the LUMO, respectively. Expectedly, the S K-edge spectrum of dinuclear DNIC **5** exhibits four well-resolved pre-edge absorption peaks (2469.1, 2470.1, 2471.1, and 2472.2 eV). In conclusion, the S K-edge pre-edge pattern/energy can serve as an efficient method to characterize the mononuclear DNICs and the dinuclear DNICs containing bridged-thiolate and bridged-sulfide ligands.

(2) The Fe−S bond covalency of mononucelar DNICs **2-Et** (82%), **2-Ph** (57%), and $[(-SC_7H_4SN)_2Fe(NO)_2]^-$ (20%) derived from the intensity of the S K-edge pre-edge absorption rationalizes the Fe−S bond distances following the trend of $[(-SC_7H_4SN)_2Fe(NO)_2]^-$ > **2-Ph** > **2-Et** and the binding preference of the $\{Fe(NO)_2\}^9$ core toward thiolates following the trend of $[SEt]^-$ > $[SPh]^-$ > $[SC_7H_4SN]^-$. Also, the higher Fe−S bond covalency modulated by the stronger electron-donating thiolate ligand stabilizes the $\{Fe(NO)_2\}$ core of $\{Fe(NO)_2\}^9$ DNICs and promotes Fe → NO π-electron back-donation to strengthen Fe−NO bonds and to weaken the NO-release ability, which is supported by the Raman ν(Fe−NO) stretching frequency.

(3) On the basis of the lower intensity of the first S K-edge pre-edge absorption peak of complex **4** compared to that of complex **3**, the antibonding character of the LUMO mainly contributed from the Fe−S bond in complex **3** rationalizes the elongation of the Fe−S bond and the simultaneous increase of the S_{1s} and Fe_{3d} orbital energies upon reduction of complex **3** and also uncovers the reaction of RREs and nucleophile leading to formation of mononuclear DNICs via the bridged-thiolate cleavage reaction.

(4) Combination of S K-edge pre-edge and thiolate peak energies establishes the relative energy of the Fe_{3d} manifold orbitals and uncovers the $\{Fe^{III}(NO^-)_2\}^9$ electronic structures for complexes **2-Ph**/**2-Et**. In addition, based on the Fe K-edge pre-edge energy of complexes **5** and **6** (7113.6 eV for both complexes) lying between 7113.4 (complex **4**) and 7113.8 eV (complex **3**), the relative d-manifold energy derived from S K-edge XAS also concluded that the electronic structure of the $[\{Fe(NO)_2\}^9-\{Fe(NO)_2\}^9]$ core of complexes **5** and **6** is best described as $[\{Fe^{III}(NO^-)_2\}^9-\{Fe^{III}(NO^-)_2\}^9]$ compared to the $[\{Fe^{III}(NO^-)_2\}^9-\{Fe^{III}(NO^-)_2\}^9]$ core electronic structure of complex **3**.

Serving as the product of the NO-signaling pathway, DNICs were first identified 45 years ago via its distinct EPR signal at g = 2.03.[1,2] Recently, nuclear resonance vibrational spectroscopy (NRVS) was also employed to identify formation of the varieties of DNICs based on their characteristic vibrational frequencies.[22] In addition to probing formation of DNICs by the characteristic Fe K-edge pre-edge absorption energy ranging from 7113.4 to 7113.8 eV,[9] the distinct S K-edge pre-edge absorption energy and pattern can serve as an efficient tool to unambiguously characterize and discriminate mononuclear DNICs and dinuclear DNICs containing bridged-thiolate and bridged-sulfide ligands. Also, this study may signify that the Fe−S bond covalency of protein-bound DNICs is the key factor in regulating/determining DNICs to release the $\{Fe(NO)_2\}$ motif or nitric oxide in biology.

■ EXPERIMENTAL SECTION

Manipulations, reactions, and transfers were conducted under nitrogen according to Schlenk techniques or in a glovebox (N_2 gas). Solvents

were distilled under nitrogen from appropriate drying agents (diethyl ether from CaH_2; acetonitrile from $CaH_2-P_2O_5$; methylene chloride from CaH_2; methanol from Mg/I_2; hexane and tetrahydrofuran (THF) from sodium benzophenone) and stored in dried, N_2-filled flasks over 4 Å molecular sieves. Nitrogen was purged through these solvents before use. Solvent was transferred to the reaction vessel via stainless cannula under a positive pressure of N_2. Complexes $[PPN][(NO)Fe(SPh)_3]$,[19] $[PPN][(NO)Fe(SEt)_3]$,[19] $[PPN][(NO)_2Fe(SPh)_2]$,[5] $[PPN][(NO)_2Fe(SEt)_2]$,[19] $[PPN][(NO)_2Fe(\mu\text{-}SEt)_2Fe(NO)_2]$,[6a] $[PPN][(NO)_2Fe(\mu\text{-}SEt)(\mu\text{-}S)Fe(NO)_2]$,[6b] $[(NO)_2Fe(\mu\text{-}SEt)_2Fe(NO)_2]$, and $[PPN]_2[(NO)_2Fe(\mu\text{-}S)_2Fe(NO)_2]$ were synthesized based on the literature reported.[6]

X-ray Absorption Measurements. All X-ray absorption experiments were carried out at the National Synchrotron Radiation Research Center (NSRRC), Hsinchu, Taiwan. Both Fe and S K-edge spectra were recorded at room temperature. The spectra were reduced and normalized based on the procedures reported by Solomon and co-workers.[11b] Data were averaged, and a smooth background was removed from all spectra by fitting a straight line to the pre-edge region and subtracting this straight line from the entire spectrum. Normalization of the data was accomplished by fitting a flat polynomial to the postregion and normalizing the edge jump to 1.0 at 7400 eV for the Fe K-edge and 2550 eV for the S K-edge spectra. For Fe K-edge measurements, experiments were performed in transmission mode at the BL17C wiggler beamline with a double-crystal Si(111) monochromator. The energy resolution $\Delta E/E$ was estimated to be about 2×10^{-4}. High harmonics were rejected by Rh-coated mirrors. The spectra were scanned from 6.912 to 8.006 keV. A reference Fe foil is always measured simultaneously, in which the first inflection point at 7112.0 eV of the Fe foil spectrum is used for energy calibration. Ion chambers used to measure the incident (I_0) and transmitted (I) beam intensities were filled with a mixture of N_2 and He gases and a mixture of N_2 and Ar gases, respectively.

The S K-edge data were collected in fluorescence mode at BL 16A with a Si(111) monochromator. The energy resolution $\Delta E/E$ is 1.4×10^{-4}. The energy is scanned from 2.42 to 2.77 keV. A Lytle detector was employed for fluorescence measurements in which the sample chamber is filled with high-purity He gas to avoid air absorption. Samples were ground to powder from single crystals and secured in the bag made of 3.6-μm Mylar film. The absorption of the S K-edge region of the empty bag made of 3.6-μm Mylar film was verified to be negligible. The photon energy was calibrated to the maximum of the first pre-edge feature of $Na_2S_2O_3.5H_2O$ at 2472.02 eV.[11] The pre-edge features at the S K-edge were fitted using the software package ORIGIN and modeled by Lorentzian functions over the range of 2465−2475 eV. The % S_{3p} in the half-occupied or unoccupied orbital of complexes **2-Et**, **2-Ph**, and $[(-SC_7H_4SN)_2Fe(NO)_2]^-$ was determined using reference spectra and pre-edge fits of complex $[Fe(SPh)_4]^-$.[11] The intensity of the pre-edge feature of complex $[Fe(SPh)_4]^-$ was defined as 1.03 unit, which corresponds to 128% total covalency.[11] Since the intensity is normalized based on $[Fe(SPh)_4]^-$, the intensity of complexes **2-Et**, **2-Ph**, and $[(-SC_7H_4SN)_2Fe(NO)_2]^-$ was multiplied by a factor of 0.5. Also, the difference of the bond length among complexes $[Fe(SPh)_4]^-$, **2-Et**, **2-Ph**, and $[(-SC_7H_4SN)_2Fe(NO)_2]^-$ was taken into consideration by multiplying a fator of 2.30 Å/R_{Fe-S} Å of DNICs.[2]

It has been reported that there are several possible sources of systematic error in the analysis of these spectra.[11b] The normalization procedure can produce a 1−3% difference in the pre-edge peak heights, as determined by varying the parameters used to normalize a set of S K-edge spectra. The errors derived from the normalization (by taking the maximum 3%) and fitting procedure were combined and are reported in Table 3. The uncertainty in the pre-edge and edge energies is limited by the reproducibility of the edge spectra (∼0.35 eV for Fe K-edge and ∼0.1 eV for S K-edge). Thus, the relative energies of the features are reported with an error of ±0.35 eV for the Fe K-edge and ± 0.1 eV for the S K-edge.

TD-DFT Calculation. All TD-DFT calculations for S K-edge regions were carried out with the ORCA electronic structure package version 2.8.0.[23] The S K-edge calculation was conducted based on the procedure reported by Neese and co-worker.[24] The B3LYP exchange functional and def2-TZVP(-f) basis set on the Fe, S, N, O, C, and H atoms were used for electronic structure calculation. How the different exchange functionals influence the TD-DFT on S K-edge pre-edge regions are tested, and the better one is to mix ∼17−18% HFx (Hartree−Fock exchange). As this mixing value is close to 20% HFx in B3LYP and B3LYP also provides a similar profile to reproduce the XAS data and the same scientific meaning, we apply the B3LYP functional on all electronic calculations. All unrestricted calculations were done at C_1 symmetry, except for complex **3** (C_i symmetry was used in the calculation). Each structure has been checked without an imaginary frequency in the ORCA package. The LÖwdin population analysis was used to obtain the contributions of Fe, S, and NO on each MO. The coordinates used for geometry optimization of complex $[(-SC_7H_4SN)_2Fe(NO)_2]^-$ were based on the experimental structures taken from the X-ray diffraction experiments.[5] Geometry optimizations were done in redundant internal coordinates. The BP86 functional together with the def2-TZVP(-f) basis set were used in the geometry optimization. The coordinates used for the TD-DFT calculation of complexes **2-Et** and **2-Ph** were based on the geometry-optimized structure reported in the previous study,[9] in which the BP86 functional together with the aug-cc-pVTZP basis set on the Fe, S, N, and O atoms and the SV(P) basis set on the C and H atoms were applied. The geometry of complexes **1-Ph** and **3** was taken from X-ray diffraction experiments[6a,b] and then optimized in the Gaussian 09 package[25] with the same basis set, def2-TZVP(-f), and BP86 exchange functional. Isosurface plots of the MOs were generated using the GaussView 5.0 program with an isovalue surface at 0.04 au.

Raman Measurements. Raman spectra were recorded in a backscattering geometry to improve the signal-to-noise ratio. The spectra resolution, 3 cm^{-1}, was limited by the Spex 1877C monochromator (length 0.6 m, grating with 600 grooves/mm). A He−Ne laser (wavelength 632.8 nm) served as the excitation source; the laser power at the sample was set below 15 mW. The sample was sealed in a glass cell and kept under nitrogen. The scattered signals passing through a notch filter were recorded with a thermoelectrically cooled Roper 7430 CCD detector. All spectra were recorded under room temperature. Samples were mixed with KBr to avoid self-absorption.

■ ASSOCIATED CONTENT

Supporting Information. The estimation of oxidation state by pre-edge transition energy, S K-edge spectra of complexes **1-Ph**, **2-Ph**, **1-Et**, and **2-Et**, the unoccupied MO diagram of complex **2-Ph**, and the TD-DFT calculated pre-edge absorption of complexes **2-Ph** as well as $[(-SC_7H_4SN)_2Fe(NO)_2]^-$. This material is available free of charge via the Internet at http://pubs.acs.org.

■ AUTHOR INFORMATION

Corresponding Author
*E-mail: wfliaw@mx.nthu.edu.tw.

■ ACKNOWLEDGMENT

We gratefully acknowledge financial support from the National Science Council of Taiwan. We also thank NSRRC and NCHC for their support on the hardware and software applied in this work.

REFERENCES

(1) (a) Ueno, T.; Susuki, Y.; Fujii, S.; Vanin, A. F.; Yoshimura, T. *Biochem. Pharmacol.* **2002**, *63*, 485–493. (b) Frederik, A. C.; Wiegant, I. Y.; Malyshev, I. Y.; Kleschyov, A. L.; van Faassen, E.; Vanin, A. F. *FEBS Lett.* **1999**, *455*, 179–182.

(2) (a) Foster, M. W.; Cowan, J. A. *J. Am. Chem. Soc.* **1999**, *121*, 4093. (b) Cooper, C. E. *Biochim. Biophys. Acta* **1999**, *1411*, 290–309.

(3) (a) Boese, M.; Mordvintcev, P. I.; Vanin, A. F.; Busse, R.; Mülsch, A. *J. Biol. Chem.* **1995**, *270*, 29244–29249. (b) Vanin, A. F. *FEBS Lett.* **1991**, *1*, 1–3. (c) Giannone, G.; Takeda, K.; Kleschyov, A. L. *J. Physiol.* **2000**, *529*, 735–745. (d) Badorff, C.; Fichtlscherer, B.; Muelsch, A.; Zeiher, M. A.; Dimmeler, S. *Nitric Oxide* **2002**, *6*, 305–312. (e) Severina, I. S.; Bussygina, G. O.; Pyatakova, V. N.; Malenkova, V. I.; Vanin, A. F. *Nitric Oxide* **2003**, *8*, 155–163. (f) Vasil'eva, S. V.; Osipov, A. N.; Sanina, N. A.; Aldoshin, S. M. *Biochem. Biophys.* **2007**, *414*, 102–105. (g) Kleschyov, A. L.; Strand, S.; Schmitt, S.; Gottfried, D.; Skatchkov, M.; Sjakste, N.; Daiber, A.; Umansky, V.; Munzel, T. *Free Radical Biol. Med.* **2006**, *40*, 1340–1348.

(4) (a) Cruz-Ramos, H.; Crack, J.; Wu, G.; Hughes, N. M.; Scott, C.; Thomson, J. A.; Green, J.; Poole, K. R. *EMBO J.* **2002**, *21*, 3235–3244. (b) Tinberg, C. E.; Tonzetich, Z. J.; Wang, H.; Do, L. H.; Yoda, Y.; Cramer, S. P.; Lippard, S. J. *J. Am. Chem. Soc.* **2010**, *132*, 18168–18176.

(5) Tsai, F.-T.; Chiou, S.-J.; Tsai, M.-C.; Tsai, M.-L.; Huang, H.-W.; Chiang, M.-H.; Liaw, W.-F. *Inorg. Chem.* **2005**, *44*, 5872–5881.

(6) (a) Lu, T.-T.; Tsou, C.-C.; Huang, H.-W.; Hsu, I.-J.; Chen, J.-M.; Kuo, T.-S.; Wang, Y.; Liaw, W.-F. *Inorg. Chem.* **2008**, *47*, 6040–6050. (b) Lu, T.-T; Huang, H.-W.; Liaw, W.-F. *Inorg. Chem.* **2009**, *48*, 9027–9035. (c) Conradie, J.; Quarless, D. A.; Hsu, H. F.; Harrop, T. C.; Lippard, S. J.; Koch, S. A.; Ghosh, A. *J. Am. Chem. Soc.* **2007**, *129*, 10446–10456. (d) Ghosh, A. *J. Inorg. Biochem.* **2005**, *99*, vi–viii. (e) Brown, C. A.; Pavovski, M. A.; Westre, T. E.; Zhang, Y.; Hedman, B.; Hodgson, K. O.; Solomon, E. I. *J. Am. Chem. Soc.* **1995**, *117*, 715–732. (f) Schenk, G.; Pau, M. Y. M.; Solomon, E. I. *J. Am. Chem. Soc.* **2004**, *126*, 505–515.

(7) Tsou, C.-C.; Lu, T.-T.; Liaw, W.-F. *J. Am. Chem. Soc.* **2007**, *129*, 12626–12627.

(8) Tsai, M.-L.; Liaw, W.-F. *Inorg. Chem.* **2006**, *45*, 6583–6585.

(9) Tsai, M.-C.; Tsai, F.-T.; Lu, T.-T.; Tsai, M.-L.; Wei, Y.-C.; Hsu, I.-J.; Lee, J.-F.; Liaw, W.-F. *Inorg. Chem.* **2009**, *48*, 9579–9591.

(10) Ye, S.; Neese, F. *J. Am. Chem. Soc.* **2010**, *132*, 3646–3647.

(11) (a) Glaser, T.; Hedman, B.; Hodgson, K. O.; Solomon, E. I. *Acc. Chem. Res.* **2000**, *33*, 859–868. (b) Solomon, E. I.; Hedman, B.; Hodgson, K. O.; Dey, A.; Szilagyi, R. K. *Coord. Chem. Rev.* **2005**, *249*, 97–129. (c) Rompel, A.; Cinco, R. M.; Latimer, M. J.; McDermott, A. E.; Guiles, R. D.; Quitanilha, A.; Krauss, R. M.; Sauer, K.; Yachandra, V. K.; Klein, M. P. *Proc. Natl. Acad. Sci.* **1998**, *95*, 6122–6127. (d) Pickering, I. J.; Prince, R. C.; Divers, T.; George, D. N. *FEBS Lett.* **1998**, *441*, 11–14. (e) Szilagyi, R. K.; Schwab, D. E. *Biochem. Biophys. Res. Commun.* **2005**, *330*, 60–64. (f) Martin-Diaconescu, V.; Kennepohl, P. *J. Am. Chem. Soc.* **2007**, *129*, 3034–3035. (g) Tenderholt, A. L.; Wang, J.-J.; Szilagyi, R. K.; Holm, R. H.; Hodgson, K. O.; Hedman, B.; Solomon, E. I. *J. Am. Chem. Soc.* **2010**, *132*, 8359–8371. (h) Rose, K.; Shadle, S. E.; Eidsness, M. K.; Kurtz, D. M., Jr.; Scott, R. A.; Hedman, B.; Hodgson, K. O.; Solomon, E. I. *J. Am. Chem. Soc.* **1998**, *120*, 10743–10747.

(12) (a) Sriskandakumar, T.; Petzold, H.; Bruijnincx, P. C. A.; Habtemariam, A.; Sadler, P. J.; Kennepohl, P. *J. Am. Chem. Soc.* **2009**, *131*, 13355–13361. (b) Doonan, C. J.; Rubie, N. D.; Peariso, K.; Harris, H. H.; Knottenbelt, S. Z.; George, G. N.; Young, C. G.; Kirk, M. L. *J. Am. Chem. Soc.* **2008**, *130*, 55–65. (c) Laughlin, L. J.; Eagle, A. A.; George, G. N.; Tiekink, E. R. T.; Young, C. G. *Inorg. Chem.* **2007**, *46*, 939–948.

(13) (a) Dey, A.; Chow, M.; Taniguchi, K.; Lugo-Mas, P.; Davin, S.; Maeda, M.; Kovacs, J. A.; Odaka, M.; Hodgson, K. O.; Hedman, B.; Solomon, E. I. *J. Am. Chem. Soc.* **2006**, *128*, 533–541. (b) Dey, A.; Jeffrey, S. P.; Darensbourg, M.; Hodgson, K. O.; Hedman, B.; Solomon, E. I. *Inorg. Chem.* **2007**, *46*, 4989–4996. (c) Lugo-Mas, P.; Dey, A.; Xu, L.; Davin, S. D.; Benedict, J.; Kaminsky, W.; Hodgson, K. O.; Hedman, B.; Solomon, E. I.; Kovacs, J. A. *J. Am. Chem. Soc.* **2006**, *128*, 11211–11221.

(14) (a) Szilagyi, R. K.; Bryngelson, P. A.; Maroney, M. J.; Hedman, B.; Hodgson, K. O.; Solomon, E. I. *J. Am. Chem. Soc.* **2004**, *126*, 3018–3019. (b) Shearer, J.; Dehestanl, A.; Abanda, F. *Inorg. Chem.* **2008**, *47*, 2649–2660.

(15) (a) Dey, A.; Jiang, Y.; de Montellano, P. O.; Hodgson, K. O.; Hedman, B.; Solomon, E. I. *J. Am. Chem. Soc.* **2009**, *131*, 7869–7878. (b) Dey, A.; Okamura, T.; Ueyama, N.; Hedman, B.; Hodgson, K. O.; Solomon, E. I. *J. Am. Chem. Soc.* **2005**, *127*, 12046–12053.

(16) Dey, A.; Jenney, F. E., Jr.; Adams, M. W. W.; Babini, E.; Takahashi, Y.; Fukuyama, K.; Hodgson, K. O.; Hedman, B.; Solomon, E. I. *Science* **2007**, *318*, 1464–1468.

(17) (a) Glaser, T.; Rose, K.; Shadle, S. E.; Hedman, B.; Hodgson, K. O.; Solomon, E. I. *J. Am. Chem. Soc.* **2001**, *123*, 442–454. (b) Shadle, S. E.; Hedman, B.; Hodgson, K. O.; Solomon, E. I. *Inorg. Chem.* **1994**, *33*, 4235–4244. (c) Sun, N.; Liu, L. V.; Dey, A.; Villar-Acevedo, G.; Kovacs, J. A.; Darensbourg, M. Y.; Hodgson, K. O.; Hedman, B.; Solomon, E. *Inorg. Chem.* **2011**, *50*, 427–436. (d) Shadle, S. E.; Hedman, B.; Hodgson, K. O.; Solomon, E. I. *J. Am. Chem. Soc.* **1995**, *117*, 2259–2272.

(18) Rose, K.; Shadle, S. E.; Glaser, T.; de Vries, S.; Cherepanov, A.; Canters, G. W.; Hedman, B.; Hodgson, K. O.; Solomon, E. I. *J. Am. Chem. Soc.* **1999**, *121*, 2353–2363.

(19) Lu, T.-T.; Chiou, S.-J.; Chen, C.-Y.; Liaw, W.-F. *Inorg. Chem.* **2006**, *45*, 8799–8806.

(20) Strasdeit, H.; Krebs, B.; Henkel, G. *Z. Naturforsch.* **1986**, *41b*, 1357–1362.

(21) Dai, R. J.; Ke, S. C. *J. Phys. Chem. B* **2007**, *111*, 2335–2346.

(22) Tonzetich, Z. J.; Wang, H.; Mitra, D.; Tinberg, C. E.; Do, L. H.; Jenney, F. E., Jr.; Adams, M. W. W.; Cramer, S. P.; Lippard, S. J. *J. Am. Chem. Soc.* **2010**, *132*, 6914–6916.

(23) Neese, F. *ORCA-an ab Initio, Density functional and Semiempirical Electronic Structure Package*, version 2.8.0; University of Bonn: Germany, 2010.

(24) George, S. D.; Neese, F. *Inorg. Chem.* **2010**, *49*, 1849–1853.

(25) Frisch, M. J.; et al. *Gaussian 09*, revision A.02; Gaussian, Inc.: Wallingford, CT, 2009.

(26) DenningtonII, R.; Keith, T.; Millam, J. *GaussView*, version 5.0, SemiChem. Inc:. Shawnee Mission, KS, 2009.